RESEARCH ARTICLE

Effects of miR-219/miR-338 on microglia and astrocyte behaviors and astrocyte-oligodendrocyte precursor cell interactions

Lan Huong Nguyen[1, †], William Ong[1], Kai Wang[1], Mingfeng Wang[1], Dean Nizetic[2, 3], Sing Yian Chew[1, 2, *]
1 School of Chemical and Biomedical Engineering, Nanyang Technological University, Singapore, Singapore
2 Lee Kong Chian School of Medicine, Nanyang Technological University, Singapore, Singapore
3 Blizard Institute, Barts & The London School of Medicine, Queen Mary University of London, London, UK

Funding: *This work was supported by the Singapore National Research Foundation under its NMRC-CBRG grants (Project award number: NMRC/CBRG/0096/2015) and administered by the Singapore Ministry of Health's National Medical Research Council and partially supported by the MOE Academic Research Funding (AcRF) Tier 1 grant (RG148/14) and Tier 2 grant (MOE2015-T2-1-023).*

Abstract

MiR-219 and miR-338 (miR-219/miR-338) are oligodendrocyte-specific microRNAs. The overexpression of these miRs in oligodendrocyte precursor cells promotes their differentiation and maturation into oligodendrocytes, which may enhance axonal remyelination after nerve injuries in the central nervous system (CNS). As such, the delivery of miR-219/miR-338 to the CNS to promote oligodendrocyte precursor cell differentiation, maturation and myelination could be a promising approach for nerve repair. However, nerve injuries in the CNS also involve other cell types, such as microglia and astrocytes. Herein, we investigated the effects of miR-219/miR-338 treatment on microglia and astrocytes *in vitro* and *in vivo*. We found that miR-219/miR-338 diminished microglial expression of pro-inflammatory cytokines and suppressed astrocyte activation. In addition, we showed that miR-219/miR-338 enhanced oligodendrocyte precursor cell differentiation and maturation in a scratch assay paradigm that re-created a nerve injury condition *in vitro*. Collectively, our results suggest miR-219/miR-338 as a promising treatment for axonal remyelination in the CNS following nerve injuries. All experimental procedures were approved by the Institutional Animal Care and Use Committee (IACUC), Nanyang Technological University (approval No. A0309 and A0333) on April 27, 2016 and October 8, 2016.

Key Words: *central nervous system; electrospinning; gene silencing; glia; hydrogel; myelination; nanofibers; oligodendroglial; polycaprolactone; spinal cord injury*

Chinese Library Classification No. *R459.9; R364; Q2*

***Correspondence to:**
Sing Yian Chew, PhD,
sychew@ntu.edu.sg.

†Current address:
NUS Synthetic Biology for Clinical and Technological Innovation (SynCTI), Life Sciences Institute, National University of Singapore, Singapore

orcid:
0000-0002-6084-5967
(Sing Yian Chew)

doi: *10.4103/1673-5374.266922*

Received: *June 15, 2019*
Peer-review started: *June 21, 2019*
Accepted: *September 12, 2019*
Published online: *October 18, 2019*

Introduction

MicroRNAs (miRs) are post-transcriptional regulators. They prevent translation or trigger degradation to inhibit protein expression (Ambros, 2004; Bartel, 2004). A single miR can silent an extensive network of downstream targets since miRs are only needed to be partially complementary to their target mRNAs (Lam et al., 2015). Therefore, RNA interference using miRs offers a potent therapeutic strategy.

MiR-219 and miR-338 (miR-219/miR-338) are highly expressed in oligodendrocytes (OLs) (Dugas et al., 2010; Zhao et al., 2010). They regulate oligodendrocyte development by targeting negative regulators of OL differentiation (Zhao et al., 2010; Galloway and Moore, 2016). Transfection of miR-219/miR-338 into mouse OL precursor cells (OPCs) enhanced the percentage of myelinating OLs by 5.1-fold (Zhao et al., 2010). Meanwhile, *in vitro* fiber-mediated reverse transfection of miR-219/miR-338 improved OL maturation by 5-fold (Diao et al., 2015b). Furthermore, these miRs have a crucial role in the formation and maintenance of myelin. Mir-219 delivery enhanced remyelination and promoted functional recovery in multiple sclerosis rodent models, while the deletion of miR-338 in miR-219-deficient mice exacerbated the dysmyelination phenotype (Wang et al., 2017). Our recent study also showed that rats implanted with miR-219/miR-338-loaded scaffolds possessed a higher number of oligodendroglial lineage cells and a formation of more compact myelin sheaths post-spinal cord injuries (SCI) (Milbreta et al., 2018).

OLs are highly vulnerable to cell necrosis after nerve injuries (Almad et al., 2011; Alizadeh et al., 2015). Their loss causes axon demyelination, which further exacerbates nerve degeneration. Correspondingly, the proliferation rate of OPCs increases markedly after nerve injuries to compensate for OL loss (Almad et al., 2011; Li and Leung, 2015). Despite such spontaneous response, remyelination remains sub-optimal, possibly because these OPCs cannot differentiate and mature into myelinating OLs (Jiang et al., 2008; Alizadeh et al., 2015). Thus, the delivery of miR-219/miR-338 to the CNS to promote OPC differentiation, maturation, and myelination may be a promising treatment for nerve injuries.

However, biological responses following injuries in the CNS are complicated and involve many cell types besides OPCs. Upon injuries, microglia and astrocytes are activated and undergo dramatic alteration in morphology, expression of cell surface molecules and release of cytokines (Hausmann, 2003; Markiewicz and Lukomska, 2006; Lull and Block, 2010). The activation of these cells is beneficial and detrimental on nerve repair concurrently (Loane and Byrnes,

2010; Burda et al., 2016). In addition, astrocyte reactivity also influences the development of OL lineage and remyelination (Clemente et al., 2013; Domingues et al., 2016). Therefore, it is critical to look at the effects of miR-219/miR-338 on other glia cells before employing these miRs as therapeutics.

Here, we investigated the effects of miR-219/miR-338 on gene silencing and activation of microglia and astrocytes *in vitro* and *in vivo*. A hemi-incision model at C5 level of the rat spinal cord was chosen as a proof-of-concept for nerve injuries in the CNS (**Figure 1A**). We also examined the effects of miR-219/miR-338 on OL maturation *in vitro*, in the context of an injured astrocyte-OPC co-culture, an injury mimicking condition.

Materials and Methods

Scaffold fabrication

Aligned poly (ε-caprolactone-co-ethyl ethylene phosphate) (PCLEEP) fiber-hydrogel scaffold for in vivo implantation

The aligned PCLEEP copolymer (M_w = 40,509, M_n = 17,288) was synthesized according to a previous method (Wang et al., 2009). Thereafter, PCLEEP (25% wt%) was dissolved in 2, 2, 2-trifluoroethanol (TFE, ≥ 99.0 %, Sigma, St. Louis, MO, USA) and electrospun via the two-pole air gap electrospinning method (Jha et al., 2011). Briefly, after loading into a syringe, the PCLEEP polymer solution was charged at +10 kV and dispensed at a flow rate of 1.9 mL/h. Thereafter, the PCLEEP fibers were formed and deposited between two stationary collector poles (–5.0 kV) bridging a 5.0 cm air gap area. Every set of aligned PCLEEP fibers was retrieved after 1 minute of electrospinning. Following that, the fibers were sterilized under ultraviolet light for 30 minutes.

The aligned PCLEEP fiber-hydrogel scaffolds were fabricated according to our reported method (Nguyen et al., 2017; Milbreta et al., 2018). Briefly, a cylindrical mold (5.0 mm in length and 4.5 mm in inner diameter) was sterilized and pre-set with four bundles of PCLEEP fibers. Meanwhile, rat-tail collagen type I (10.08 mg/mL, Corning, Corning, NY, USA) was mixed with 10× phosphate-buffered saline (10× PBS, Thermo Fisher Scientific, Waltham, MA, USA), 1.0 N NaOH (Sigma), and deionized water (DI) water to obtain a final collagen concentration of 6.0 mg/mL. For miR incorporation, miRs (100 μM, Thermo Fisher Scientific) (3.75 μL of negative control (NEG)-miR or 7.5 μL of a mixture of miR-219, miR-338-3p, and miR-338-5p with equal volume) and 7.5 μL of TransIT-TKO (MirusBio, Madison, WI, USA) were complexed for 15 minutes and then added into 100 μL of the collagen mixture in place of DI water. To obtain scaffolds with aligned nanofibers, the collagen mixture was added into the pre-set mold and then incubated at 37°C for 45 minutes to enable hydrogel formation. Following that, the scaffolds were frozen at –80°C, lyophilized overnight, and then kept at –20°C until further experiments.

Aligned PCL-DPP-PCL fibers for in vitro experiments

The fluorescent poly (ε-caprolactone) polymer (denoted as PCL-DPP-PCL) (average M_n = 38,300 g/mol, M_w/M_n = 2.0) was synthesized according to the previously reported method (Wang et al., 2015). To fabricate aligned fibers, poly (ε-caprolactone) (PCL, 12 wt%, Sigma) and PCL-DPP-PCL (2 wt%) polymers were dissolved together in TFE. After loading into a syringe that was capped with a blunt needle (22-gauge), the copolymer solution was electrically charged at +10 kV and dispensed at 1.5 mL/h. The aligned fibers were then deposited onto a negatively charged rotating target (–4 kV, 525 × *g*) that was set at a distance of 14 cm. Thereafter, the scaffolds were punched into circular shapes with a diameter of 16 mm to fit 24-well tissue culture plates for downstream cellular studies.

Poly-DOPA and PDL coatings of PCL-DPP-PCL scaffolds

PCL-DPP-PCL scaffolds were pre-wet with 70% ethanol followed by DI water. Thereafter, they were incubated in 0.5 mg/mL of 3,4-dihydroxy-L-phenylalanine (DOPA, Sigma), which was dissolved in poly-DOPA coating buffer that comprised of 10 mM Bicine (Sigma) and 250 mM NaCl (pH 8.5, Sigma) for 4 hours at 150 r/min. The scaffolds were then washed with DI water three times, 30 min/time and lyophilized overnight. Subsequently, they were incubated in poly-D-lysine solution (PDL, 5.0 μg/mL, Sigma) at 37°C and 100 r/min overnight. On the next day, the scaffolds were washed twice with PBS (10010-023, Thermo Fisher Scientific) for 15 minutes each time and then immersed in Dulbecco's modified Eagle's medium (DMEM, 11960-044, Thermo Fisher Scientific) until cell seeding.

Scaffold characterization

The aligned PCL-DPP-PCL fibers and aligned PCLEEP fiber-collagen hydrogel scaffolds were sputter-coated with platinum (JFC-1600; JEOL, Akishima, Tokyo, Japan) at 10 mA for 120 and 140 seconds, respectively. Thereafter, the samples were examined using a scanning electron microscope (JEOL, JSM-6390 LA) at an accelerating voltage of 10 kV. Following that, fiber diameters were quantified using the ImageJ software (http://imagej.nih.gov/ij/) on scanning electron microscope images, with at least 100 fibers being measured. In addition, the aligned PCL-DPP-PCL fibers were also examined and imaged using a Zeiss LSM 800 inverted confocal microscope (Carl Zeiss Pte. Ltd., Singapore).

Preparation of poly-L-lysine solution-coated coverslips for microglia culture

Glass coverslips (13 mm diameter) were incubated in poly-L-lysine solution (40 μg/mL, Sigma) for 1.5 hours at 37°C. Thereafter, the coverslips were washed with sterile DI water three times, air-dried, and kept at room temperature until use.

Animals

Adult female (6–8 weeks old, 200–250 g, n = 6) and time-pregnant Sprague-Dawley rats (n = 10) were purchased from In Vivos Pte Ltd. (Singapore). All experimental procedures were approved by the Institutional Animal Care and Use Committee (IACUC), Nanyang Technological University (approval No. A0309 and A0333) on April 27, 2016 and

October 8, 2016.

SCIs and scaffold implantation

SCI was performed according to our reported protocol (Nguyen et al., 2017; Milbreta et al., 2018). Briefly, the rats were anesthetized with an intraperitoneal injection of a ketamine (73 mg/kg) and xylazine (7.3 mg/kg) cocktail. Following that, a 1/3 incision was created at C5 level on the right side of the spinal cord (**Figure 1A**). Thereafter, a 1.0-mm long scaffold was implanted into the lesion site so that its aligned fibers were arranged parallel to the long axis of the spinal cord. Animals were divided into two treatment groups randomly: NEG-miR group (n = 3) and miR-219/miR-338 group (n = 3). At day 4 post-implantation, rats were anesthetized and a 4-mm portion of the spinal cord, including the injury site was taken out (**Figure 1A**) and kept in ice-cold Hanks' Balanced Salt solution (HBSS, Thermo Fisher Scientific). These spinal cord samples were then lysed and total RNAs were isolated for PCR within 1 hour of retrieval.

Primary cell isolation and culture

Cells from P1–2 neonatal rat cortices were isolated according to our reported protocol (Diao et al., 2015a) and then seeded

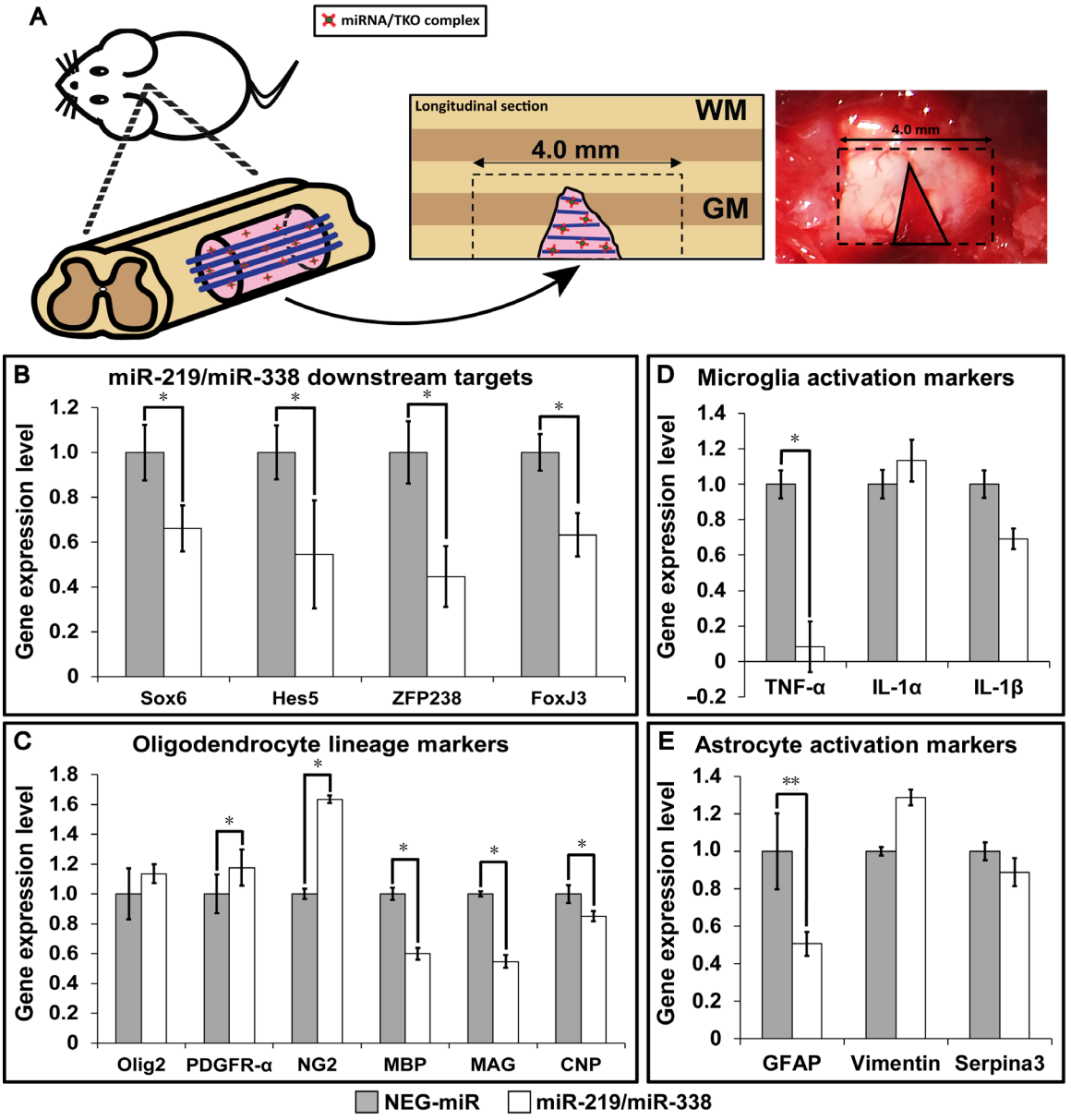

Figure 1 Effects of miR-219/miR-338 on gene expression at 4 days post-implantation *in vivo*.

(A) Schematic illustration and photograph of the *in vivo* spinal cord samples (dashed rectangle) with scaffold implantation (solid triangle), which were collected for PCR. Real-time PCR results of (B) miR-218/miR-338 downstream targets; (C) oligodendroglial, oligodendrocyte precursor cell and oligodendrocyte markers; (D) microglia activation markers and (E) astrocyte activation markers. Data are presented as the mean ± SD. $*P < 0.05$, $**P < 0.01$ (n = 3; Student's t-test). CNP: 2′,3′-Cyclic nucleotide 3′-phosphodiesterase; GFAP: glial fibrillary acidic protein; GM: gray matter; IL: interleukin; MAG: myelin-associated glycoprotein; MBP: myelin basic protein; NG2: neural/glial antigen 2; Olig2: oligodendrocyte transcription factor; PDGFR: platelet-derived growth factor receptor; TNF: tumor necrosis factor; WM: white matter.

in T75 flasks (1×10^7 cells/flask, Corning). DMEM20S medium, which consisted of DMEM, 20 % fetal bovine serum (FBS, 11995-065, Thermo Fisher Scientific), 4 mM L-glutamine (G8540, Sigma), 1 mM sodium pyruvate (P2258, Sigma), 50 U/mL penicilin and 50 μg/mL streptomycin (P/S, 15140-122, Thermo Fisher Scientific), was used and replaced every 3 days. After 10 days, the flasks were shaken at 37°C, 250 r/min for 30 minutes to isolate microglia. The purified microglia were then seeded onto the poly-L-lysine solution-coated coverslips (20,000 cells/coverslip) and cultured in glial medium that comprised of DMEM GlutaMAX (10569-010, Thermo Fisher Scientific), 10 % FBS, and 1 % P/S.

After harvesting microglia, the flasks were added with fresh DMEM20S medium and then re-shaken at 37°C, 200 r/min for 18–20 hours. Following that, the cell suspension was collected and filtered through a 20 μm sterile screening pouch (Sefar Inc., Depew, NY, USA). The purified OPCs in the flowthrough were seeded onto the DOPA-PDL coated PCL-DPP-PCL scaffolds (50,000 cells/scaffold) and cultured in DMEM high glucose (11995065, Thermo Fisher Scientific) supplemented with modified SATO (Bechler et al., 2015), 1% P/S, insulin-transferrin-sodium selenite liquid media supplement (ITS, Sigma), 0.5% FBS, and freshly prepared 10 ng/mL of platelet-derived growth factor-AA (PDGF-AA, 100-13A, PeproTech, Rocky Hill, NJ, USA) and 10 ng/mL of fibroblast growth factor-basic (100-18B, PeproTech). On the next day, scaffolds were flipped over and placed on top of the injured astrocyte cultures as shown in **Figure 2E** for the injured astrocyte-OPC co-cultures.

The remaining flasks, after replaced with the glial medium, were further shaken for 6–8 hours at 37°C, 250 r/min to remove residual OPCs. The medium was then discarded, and the flasks were rinsed with PBS and trypsinized by 0.25% Trypsin (25200-072, Thermo Fisher Scientific) for 5 minutes to isolate astrocytes. The astrocytes were seeded onto 13 mm glass coverslips at a density of 20,000 or 50,000 cells/coverslip for astrocyte and scratch assay cultures respectively. All cultures were then maintained in glial medium.

MiR transfection

TKO with equal volume of miR-219/miR-338 were complexed in DMEM for 15 minutes. At 24 hours after cell seeding, 100 μL of the miR/TKO complexes was added into each well. After initial optimization, miR:TKO volume ratio 1:1 (0.25 μL miRs (100 μM)/well) was chosen for all *in vitro* experiments since this condition did not affect cell viability and it was also the ratio used in the *in vivo* study.

Cell viability assay

At 2 days post-transfection, three coverslips from three independent cultures for each experimental group were collected and live-dead assay was conducted using the LIVE/DEAD® cell viability kit (Thermo Fisher Scientific) following the manufacturer's protocol. All samples were examined and captured via a Leica DMi8 inverted microscope and ImageJ software was used to quantify the images. For each group, at least 500 cells were quantified.

Immunocytochemistry

At indicated time points, coverslips and scaffolds were fixed with 4% ice-cold paraformaldehyde (Millipore, Burlington, MA, USA). Thereafter, the samples were permeabilized with 0.3% Triton X-100 (Sigma) in PBS for 15 minutes and then blocked in 10% normal goat serum (Sigma) for 1 hour. Subsequently, the samples were incubated with primary antibodies that were diluted in 5% normal goat serum at 4°C overnight followed by secondary antibodies, which were diluted in PBS for 1.5 hours. The secondary antibodies, including Alexa Fluor 488-conjugated goat anti-rabbit/rat IgG (1:500 dilution), Alexa Fluor 555-conjugated goat anti-mouse IgG (1:1000 dilution), and Alexa Fluor 633-conjugated goat anti-rabbit IgG (1:500 dilution), were obtained from Invitrogen (Carlsbad, CA, USA). DAPI (1:1000 dilution, Thermo Fisher Scientific) was used for nuclear staining. All samples were then mounted and examined using the Leica DMi8 inverted microscope (Leica Microsystems (SEA) Pte. Ltd., Singapore) and the Zeiss LSM800 inverted confocal microscope.

Evaluation of cell purity

After 24 hours of culture, the purity of isolated OPCs, microglia, and astrocytes was verified by neural/glial antigen 2 (NG2), Ox-42, and glial fibrillary acidic protein (GFAP) immunofluorescent staining, respectively. Rabbit anti-NG2 (1:200 dilution) and mouse anti-Ox-42 (1:200 dilution) were procured from Millipore. Rabbit anti-GFAP (1:2000 dilution) was purchased from Dako, Glostrup, Denmark. Immunofluorescent staining followed the methods described in the immunocytochemistry section.

Evaluation of cell morphology

At 4 days post-transfection, microglia and astrocytes were fixed and stained with Ox-42/DAPI and GFAP/DAPI, respectively. Immunofluorescent staining followed the methods described in the immunocytochemistry section. Cell morphology was then evaluated using the Leica DMi8 inverted microscope at magnifications of 10× and 20×.

Injured astrocyte-OPC co-culture

Astrocytes were cultured until confluent (8–10 days) and scratched with two glass pipettes held together at a fixed distance of 0.5 cm apart (**Figure 2E**). OPC-seeded scaffolds were flipped over and placed on top of the injured astrocyte culture immediately after the astrocytes were scratched (**Figure 2E**). The co-cultures were then transfected using the same protocol as stated above. The co-cultures were fixed for immunostaining at 4 and 7 days after transfection. The proportion of MBP-positive mature OLs was expressed as a percentage of oligodendrocyte transcription factor (Olig2)-positive oligodendroglial lineage cells. Rat anti-MBP (1:100 dilution) and rabbit anti-Olig2 (1:500 dilution) were obtained from Millipore. At least 200 Olig2-positive cells were counted for each group.

Real-time PCR

Spinal cords and cells were lysed by Trizol® (Sigma). RNA

was then extracted and reverse transcription was carried out using M-MLV transcriptase (Promega, Madison, WI, USA) according to manufacturers' protocols. Thereafter, real-time PCR was conducted using the iQ SYBR Green Supermix (Bio-Rad, Hercules, CA, USA) in a StepOnePlus™ system (Applied Biosystems, Foster City, CA, USA). The following program was used: 10 minutes at 95°C, 15 seconds at 95°C followed by 1 minute at 59°C for 40 cycles. Primers were purchased from Integrated DNA Technologies Pte. Ltd., Singapore. The sequences of the primers that were used are shown in **Additional Table 1**. Since all the primers displayed similar amplification efficiencies under the parameters used, the ΔΔCt method (Livak and Schmittgen, 2001) was adopted for analysis of fold change. Finally, the Neg-miR group was used to normalize all the results.

Statistical analysis

All results are presented as mean ± SD. The Student's *t*-test was used to analyze the results between two groups or of a group at two different time points. When samples had equal variances, the variations between groups were examined using one-way analysis of variance followed by the Turkey's *post hoc* test. Otherwise, the Kruskal-Wallis and Mann-Whitney *U* tests were utilized. A P-value ≤ 0.05 was considered statistically significant.

Results

Evaluation of gene expression after *in vivo* scaffold implantation

MiR-219/miR-338-encapsulated scaffolds downregulate downstream targets of delivered miRs

Sox6, Hes5, ZFP238, and FoxJ3 are downstream targets of miR-219 and miR-338 (Dugas et al., 2010; Zhao et al., 2010). Our results showed that at 4 days after implantation of the miR-219/miR-338-encapsulated scaffolds post-SCI, the expression of all these four targets was silenced (**Figure 1B**).

MiR-219/miR-338-encapsulated scaffolds promote OPC marker expression

To investigate the effects of miR-219/miR-338 on oligodendroglial development, we evaluated the levels of gene expression of oligodendroglial lineage marker (Olig2) (Lu et al., 2000; Zhou et al., 2000), OPC markers (PDGFR-α (Gallo and Chew, 2009) and NG2 (Kucharova and Stallcup, 2010)) and OL markers (CNP (2′,3′-cyclic nucleotide 3′-phosphodiesterase), MBP (myelin basic protein), and MAG (myelin-associated glycoprotein) (Baumann and Pham-Dinh, 2001; van der Goes and Dijkstra, 2001). As indicated in **Figure 1C**, at 4 days post-implantation, there was no change in the expression of Olig2 among the experimental groups. Meanwhile, both PDGFR-α and NG2 were significantly up-regulated in the miR-219/miR-338 group as compared to NEG-miR treatment (1.2 *vs.* 1.0 and 1.6 *vs.* 1.0, $P \leq 0.05$). However, the expression of MBP, MAG, and CNP were decreased with miR-219/miR-338 treatment.

MiR-219/miR-338-encapsulated scaffolds repress the expression of pro-inflammatory cytokines

Microglia and astrocytes are activated in response to nerve injuries. Depending on the environmental stimuli, activated microglia may acquire a pro-inflammatory phenotype (Orihuela et al., 2016; Kirkley et al., 2017). This phenotype is often associated with the increase in expression and release of pro-inflammatory cytokines, such as TNF-α, IL-1α, and IL-1β (Lull and Block, 2010; Orihuela et al., 2016; Kirkley et al., 2017). We specifically looked into these pro-inflammatory cytokines because their production and release after SCI contribute mainly to wound healing and neuropathic pain (Zhang and An, 2007). As illustrated in **Figure 1D**, when treated with miR-219/miR-338, TNF-α was significantly down-regulated as compared to NEG-miR treatment at 4 days post-implantation (0.1 *vs.* 1.0, $P \leq 0.05$). On the other hand, the expression of IL-1α and IL-1β appeared unaltered under the experimental conditions.

MiR-219/miR-338-encapsulated scaffolds inhibit astrocyte activation in vivo

Similar to microglia, astrocytes also undergo various alterations in gene expression upon activation (Zamanian et al., 2012). In particular, GFAP, Vimentin, and Serpina3 expressions are usually up-regulated in reactive astrocytes (Eliasson et al., 1999; Zamanian et al., 2012). These reactive astrocytes form glial scar, which in turn acts as a physical barrier and inhibits axonal regeneration (Stroncek and Reichert, 2008; Kawano et al., 2012). Our results show that the expression of GFAP was reduced by half when treated with miR-219/miR-338 ($P \leq 0.01$; **Figure 1E**). In contrast, the expression of Vimentin and Serpina3 were not significantly altered.

Effects of miR-219/miR-338 on activation of glial cells *in vitro*

To gain better understanding of how miR-219/miR-338 modulate microglial and astrocyte responses, we carried out miR transfection in microglial and astrocyte cultures *in vitro*. Our results show that miR-219/miR-338 did not affect the viability of microglia and astrocytes (data not shown). Next, we evaluated the extent of cellular activation by analyzing changes in cell morphology and expression of activation markers (Eliasson et al., 1999; Lull and Block, 2010; Zamanian et al., 2012).

MiR-219/miR-338 suppressed microglia activation: As shown in **Figure 2A**, no significant difference in microglial morphology was observed among the experimental groups. Meanwhile, microglial expression of the pro-inflammatory cytokines, TNF-α, IL-1α and IL-1β, became significantly down-regulated at 4 days with miR-219/miR-338 treatment ($P \leq 0.05$; **Figure 2B**).

MiR-219/miR-338 suppressed astrocyte activation: Treatment of miR-219/miR-338 *in vitro* reduced the expression of Vimentin and Serpina3, in comparison with the NEG-miR group at 4 days post-transfection ($P \leq 0.05$) while no difference in cellular morphology was detected (**Figure 2C** and **D**).

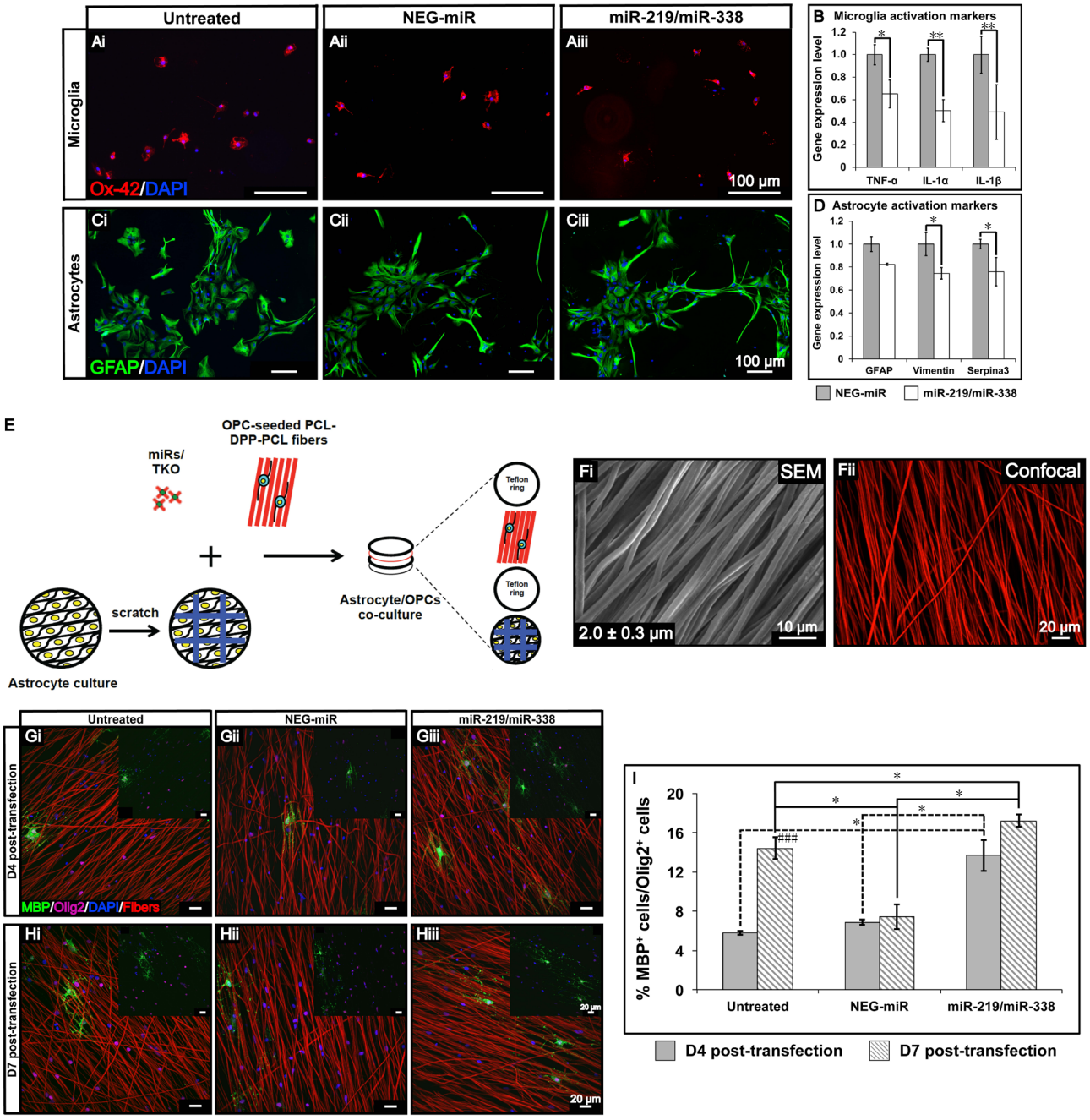

Figure 2 Effects of miR-219/miR-338 on microglia, astrocyte, and injured astrocyte-OPC co-cultures.
(A) Fluorescent micrographs of microglial in (Ai) the untreated group; (Aii) the NEG-miR group and (Aiii) the miR-219/miR-388 group. (B) Gene expression of microglia activation markers at 4 days post-transfection. Data are presented as the mean ± SD. Student's *t*-test was used. ∗$P < 0.05$, ∗∗$P < 0.01$ ($n = 3$). (C) Fluorescent micrographs of astrocytes in (Ci) the untreated group; (Cii) the NEG-miR group and (Ciii) the miR-219/miR-388 group. (D) Gene expression of astrocyte activation markers at 4 days post-transfection. Student's *t*-test was used. ∗$P < 0.05$ ($n = 3$). (E) The set-up of the injured astrocyte-OPC co-culture. (F) Images of electrospun PCL-DPP-PCL fibers taken by (Fi) SEM and (Fii) Confocal microscope at 568 nm wavelength. (G, H) Fluorescent micrographs of the co-cultures in the untreated (Gi, Hi), NEG-miR (Gii, Hii) and miR-219/miR-338 groups (Giii, Hiii). (I) Quantification of the percentage of MBP$^+$ cells at 4 and 7 days post-transfection. ∗$P < 0.05$, *vs.* other groups at the same time point (One-way analysis of variance followed by Tukey's *post hoc* test or the Kruskal-Wallis and Mann-Whitney *U* tests). ###$P < 0.001$, *vs.* the same group at 4 days ($n = 3$; Student's *t*-test). CNP: 2′,3′-Cyclic nucleotide 3′-phosphodiesterase; GFAP: glial fibrillary acidic protein; IL: interleukin; MBP: myelin basic protein; miR: microRNA; NEG-miR: negative control miR; Olig2: oligodendrocyte transcription factor; OPC: oligodendrocyte precursor cell; PCL-DPP-PCL: fluorescent poly (ε-caprolactone) polymer; SEM: scanning electron microscope; TNF: tumor necrosis factor.

OPC differentiation and maturation in the injured astrocyte-OPC co-cultures

Here, we employed PCL-DPP-PCL aligned fibers to mimic axons in OPC cultures in order to investigate only features of oligodendrocytes that are related to myelination but independent of influence from axons. As shown in **Figure 2F**, bead-free and uniformly aligned fibers with an average diameter of 2.0 ± 0.3 μm were obtained. Importantly, the

PCL-DPP-PCL fibers were highly fluorescent in a uniform manner and demonstrated robust photostability throughout the course of this study.

To assess how miR-219/miR-338 modulates oligodendrocyte differentiation in the presence of activated/injured astrocytes, we evaluated the percentage of MBP+ OLs using injured astrocyte-OPC co-cultures. As shown in **Figure 2G–I**, when OPCs and injured astrocytes were both transfected with miRs, we observed significant higher rate and extent of OL differentiation and maturation. In particular, miR-219/miR-338 transfection significantly enhanced the differentiation of OPC into MBP^+ cells as early as day 4 and this effect remained significant after 7 days of culture. Taken together, miR-219/miR-338 favored oligodendrocyte development *in vitro*.

Discussion

Nerve injuries in the CNS is often followed by axon demyelination due to a dramatic loss of OLs (Almad et al., 2011). Although there is an increase in OPC proliferation to compensate for that loss, axon remyelination remains sub-optimal due to unknown factors that inhibit OL differentiation and maturation (Jiang et al., 2008; Almad et al., 2011; Alizadeh et al., 2015). In search for possible methods to modulate remyelination, our previous work showed that miR-219/miR-338 cocktail, coupled with fiber topography, was able to enhance OL differentiation and maturation (Diao et al., 2015a, b). In addition, we developed a nanofiber platform that can provide localized and sustained delivery of drugs and nucleic acids (Nguyen et al., 2017). Using this platform, we were able to delivery miR-219/miR-338 non-virally *in vivo* and successfully enhanced remyelination post-SCI (Milbreta et al., 2018). Thus, a combining miR-219/miR-338 with our scaffold design is a potential therapeutic treatment for nerve injuries.

However, besides OPCs, the biological responses following nerve injuries in the CNS also involve microglia and astrocytes. As such, miR-219/miR-338 could possibly affect these cells, thus resulting in unascertained results upon treatment. Recently we have seen that, although our miR-291/miR-338-incoproated scaffolds remarkedly promoted remyelination within the injured CNS, no improvement on neurite outgrowth was detected (Milbreta et al., 2018). Hence, in order to optimize the miR-219/miR-338 treatment, this study was done to identify any potential effects that these miRs may have on microglia and astrocytes.

Sox6, Hes5, ZFP238, and FoxJ3 are proteins that are involved in enhancing OPC proliferation while inhibiting OL differentiation (Dugas et al., 2010; Zhao et al., 2010). Thus, by inhibiting the expression of these genes, miR-219/miR-338 promote OL differentiation (Dugas et al., 2010; Zhao et al., 2010). In this study, the implantation of miR-219/miR-338-encapsulated scaffolds resulted in the significant downregulation of all four downstream targets at 4 days post-injury. Together with our previous reports (Nguyen et al., 2017; Milbreta et al., 2018), this result further confirms the pronounced capability of our scaffold in miR delivery and gene silencing *in vivo*, while providing essential structural support and topographical signals for neotissue formation.

PDGFR-α and NG2 are widely used as OPC markers. Here, we showed that PDGFR-α and NG2 expression levels increased significantly when treated with miR-219/miR-338 in comparison with NEG-miR treatment. One possible reason for this observation may be the fact that miR-219 promotes the differentiation of neural precursor cells into OPCs, as demonstrated by Fan et al. (2017). With the success in knocking down various inhibitors of OPC differentiation, the miR-219/miR-338-incorporated scaffolds were expected to enhance OL differentiation and maturation. However, the expression levels of the middle and late OL markers (CNP, MBP, and MAG) decreased in the miR-219/miR-338 group with respect to the NEG-miR group. While the reason for this observation remains unknown, it is possible that these miRs may require more time, beyond 4 days post-injury, to exert their effects and enhance OL marker expressions. Indeed, our previous work showed that there was a significant increase in MBP expression in the miR-291/miR-338-incoproated scaffolds at 4 weeks post-implantation (Milbreta et al., 2018). Therefore, future works that aim to evaluate oligodendrocyte development should consider a long-term study of at least 4 weeks and beyond.

On the other hand, our miR-219/miR-338-incorporated scaffolds markedly decreased the expression of TNF-α at 4 days post-implantation. Furthermore, *in vitro* microglial expressions of the three pro-inflammatory cytokines, TNF-α, IL-1α, and IL-1β, were all reduced significantly at 4 days post-transfection when treated with miR-219/miR-338 while no difference in cellular morphology was detected among the experimental groups. Taken together, these results suggest that miR-219/miR-338 decreased microglia activation. Furthermore, a previous study demonstrated that treatment with an IL-1 receptor antagonist for the first 3 days after SCI in rats markedly reduced injury-induced apoptosis (Nesic et al., 2001). Thus, the use of miR-219/miR-338 may be beneficial in reducing cell death following nerve injuries.

Similar to microglia, our results showed that astrocytes were more quiescent when treated with miR-219/miR-338 since the *in vivo* expression of GFAP was significantly reduced by half at 4 days post-implantation. Moreover, treatment of miR-219/miR-338 *in vitro* also diminished the expression of Vimentin and Serpina3 when compared to the negative control group at 4 days post-transfection without affecting the cellular morphology. Altogether, our data implied that miR-219/miR-338 suppressed astrocyte activation. As such, miR-219/miR-338 treatment may be helpful in reducing glial scar formation. Moreover, by suppressing astrocyte activation, these miRs would also hinder the secretion of factors implicated in the inhibition of remyelination from reactive astrocytes, such as TNF-α, IFN-γ, hyaluronan, and ET-1 (Domingues et al., 2016; Kıray et al., 2016). However, these effects might only be temporary since there was no significant difference in GFAP protein expression between miR-219/miR-338 and NEG-miR treated groups starting 1 week post-SCI (Milbreta et al., 2018).

To study how miR-219/miR-338 modulate OPC differentiation and maturation in the injury-mimicking condition, we co-cultured OPCs with scratched astrocyte cultures. Astrocyte scratch assay has been utilized to evaluate drug efficacy on different processes during scar formation along the lesion site, including alterations in protein expression, cellular shape and migration (Höltje et al., 2005; Parmentier-Batteur et al., 2011). On the other hand, OLs require close interactions with axons for precise myelination in the CNS. Thus, it is challenging to separately examine neuronal and oligodendroglial effects on myelination in their *in vitro* co-cultures (Lee et al., 2012). To resolve this, fibers mimicking axons can be employed to investigate only features of OLs that are related to myelination. A study by Lee et al. showed that 60% of OL lineage cells ensheathed large fibers of 2.0–4.0 μm diameter, while only ~5% ensheathed 0.2–0.4 μm fibers (Lee et al., 2012). In addition, 2.0 μm aligned fibers promoted more MBP expression as compared to 300 nm or 700 nm aligned fibers (Diao et al., 2015a). Taken together, in this study, we employed highly fluorescent and photostable PCL-DPP-PCL aligned fibers with an average diameter of 2.0 ± 0.3 μm for OPC culture and visualization (Diao et al., 2016).

We evaluated the percentage of matured OL, as identified with MBP^+ signals, in the injured astrocyte-OPC co-culture. When OPCs and injured astrocytes were both transfected with miRs, we observed significantly higher rate and extent of OL differentiation and maturation. Especially, OL maturation increased by 2.3-fold as compared to the negative control at 7 days. Meanwhile, our previous study showed that when treated with miR-219/miR-338, MBP expression in OPC cultures was increased by ~2.0-fold (Diao et al., 2015b). Thus, miR-219/miR-338-transfected injured astrocytes seemed to further support the differentiation and maturation of miR-219/miR-338-transfected OPCs. Moreover, in the absence of miR-219/miR-338, miR transfection might be toxic since NEG-miR treatment significantly reduced MBP expression with respect to the untreated group at 7 days, thus highlighting the importance of the choice of miRs used for nerve injury treatment.

In conclusion, the microglia and astrocyte cellular responses towards miR-219/miR-338 were investigated in this study with the aim to provide insights to the translational applications of these miRs for the treatment of nerve injuries. Specifically, miR-219/miR-338 reduced microglial expression of pro-inflammatory cytokines and suppressed astrocyte activation both *in vivo* and *in vitro*. Furthermore, these miRs also promoted OPC maturation in the injured astrocyte-OPC co-culture. Altogether, our results suggest that miR-219/miR-338 might be further explored as a potential treatment for nerve injuries.

Acknowledgments: *We would like to thank Yanfen Peng (NTU, Singapore) for her help in confocal imaging.*
Author contributions: *LHN generated the hypothesis, designed and performed the experiments, and wrote and edited the manuscript. WO contributed to cell isolation and culture. KW and MW contributed the fluorescent PCL-DPP-PCL polymer. DN and SYC edited the manuscript and provided the funding. SYC guided the project and is the corresponding author of this manuscript. All authors approved the final version of the paper.*
Conflicts of interest: *No competing financial interests exist.*
Financial support: *This work was supported by the Singapore National Research Foundation under its NMRC-CBRG grants (Project award number: NMRC/CBRG/0096/2015) and administered by the Singapore Ministry of Health's National Medical Research Council and partially supported by the MOE Academic Research Funding (AcRF) Tier 1 grant (RG148/14) and Tier 2 grant (MOE2015-T2-1-023).*
Institutional review board statement: *All experimental procedures were approved by the Institutional Animal Care and Use Committee (IACUC), Nanyang Technological University (approval No. A0309 and A0333) on April 27, 2016 and October 8, 2016.*
Copyright license agreement: *The Copyright License Agreement has been signed by all authors before publication.*
Data sharing statement: *Datasets analyzed during the current study are available from the corresponding author on reasonable request.*
Plagiarism check: *Checked twice by iThenticate.*
Peer review: *Externally peer reviewed.*

Open peer reviewers: *He-Zuo Lü, the First Affiliated Hospital of Bengbu Medical College, China; Hua Bai, The Third Affiliated Hospital of Guiyang Medical University, China.*
Additional files:
Additional Table 1: *Sequences of primers for real time-PCR.*
Additional file 1: *Open peer review reports 1 and 2.*

References

Alizadeh A, Dyck SM, Karimi-Abdolrezaee S (2015) Myelin damage and repair in pathologic CNS: challenges and prospects. Front Mol Neurosci 8:35.

Almad A, Sahinkaya FR, McTigue DM (2011) Oligodendrocyte Fate after Spinal Cord Injury. Neurotherapeutics 8:262-273.

Ambros V (2004) The functions of animal microRNAs. Nature 431:350-355.

Bartel DP (2004) MicroRNAs: Genomics, biogenesis, mechanism, and function. Cell 116:281-297.

Baumann N, Pham-Dinh D (2001) Biology of oligodendrocyte and myelin in the mammalian central nervous system. Physiol Rev 81:871-927.

Bechler Marie E, Byrne L, ffrench-Constant C (2015) CNS myelin sheath lengths are an intrinsic property of oligodendrocytes. Curr Biol 25:2411-2416.

Burda JE, Bernstein AM, Sofroniew MV (2016) Astrocyte roles in traumatic brain injury. Exp Neurol 275:305-315.

Clemente D, Ortega MC, Melero-Jerez C, De Castro F (2013) The effect of glia-glia interactions on oligodendrocyte precursor cell biology during development and in demyelinating diseases. Front Cell Neurosci 7:268.

Diao HJ, Low WC, Lu QR, Chew SY (2015a) Topographical effects on fiber-mediated microRNA delivery to control oligodendroglial precursor cells development. Biomaterials 70:105-114.

Diao HJ, Low WC, Milbreta U, Lu QR, Chew SY (2015b) Nanofiber-mediated microRNA delivery to enhance differentiation and maturation of oligodendroglial precursor cells. J Control Release 208:85-92.

Diao HJ, Wang K, Long HY, Wang M, Chew SY (2016) Highly Fluorescent and photostable polymeric nanofibers as scaffolds for cell interfacing and long-term tracking. Adv Healthc Mater 5:529-533.

Domingues HS, Portugal CC, Socodato R, Relvas JB (2016) Oligodendrocyte, astrocyte, and microglia crosstalk in myelin development, damage, and repair. Front Cell Dev Biol 4:71.

Dugas JC, Cuellar TL, Scholze A, Ason B, Ibrahim A, Emery B, Zamanian JL, Foo LC, McManus MT, Barres BA (2010) Dicer1 and miR-219 are required for normal oligodendrocyte differentiation and myelination. Neuron 65:597-611.

Eliasson C, Sahlgren C, Berthold CH, Stakeberg J, Celis JE, Betsholtz C, Eriksson JE, Pekny M (1999) Intermediate filament protein partnership in astrocytes. J Biol Chem 274:23996-24006.

Fan HB, Chen LX, Qu XB, Ren CL, Wu XX, Dong FX, Zhang BL, Gao DS, Yao RQ (2017) Transplanted miR-219-overexpressing oligodendrocyte precursor cells promoted remyelination and improved functional recovery in a chronic demyelinated model. Sci Rep 7:41407.

Gallo V, Chew LJ (2009) Neurotransmitter and hormone receptors on oligodendrocytes and Schwann cells. In: Encyclopedia of neuroscience (Squire LR, ed), pp 1051-1059. Oxford: Academic Press.

Galloway DA, Moore CS (2016) miRNAs as emerging regulators of oligodendrocyte development and differentiation. Front Cell Dev Biol 4:59.

Hausmann ON (2003) Post-traumatic inflammation following spinal cord injury. Spinal Cord 41:369-378.

Höltje M, Hoffmann A, Hofmann F, Mucke C, Große G, Van Rooijen N, Kettenmann H, Just I, Ahnert-Hilger G (2005) Role of Rho GTPase in astrocyte morphology and migratory response during in vitro wound healing. J Neurochem 95:1237-1248.

Jha BS, Colello RJ, Bowman JR, Sell SA, Lee KD, Bigbee JW, Bowlin GL, Chow WN, Mathern BE, Simpson DG (2011) Two pole air gap electrospinning: Fabrication of highly aligned, three-dimensional scaffolds for nerve reconstruction. Acta Biomater 7:203-215.

Jiang S, Ballerini P, Buccella S, Giuliani P, Jiang C, Huang X, Rathbone MP (2008) Remyelination after chronic spinal cord injury is associated with proliferation of endogenous adult progenitor cells after systemic administration of guanosine. Purinerg Signal 4:61-71.

Kawano H, Kimura-Kuroda J, Komuta Y, Yoshioka N, Li HP, Kawamura K, Li Y, Raisman G (2012) Role of the lesion scar in the response to damage and repair of the central nervous system. Cell Tissue Res 349:169-180.

Kıray H, Lindsay SL, Hosseinzadeh S, Barnett SC (2016) The multifaceted role of astrocytes in regulating myelination. Exp Neurol 283:541-549.

Kirkley KS, Popichak KA, Afzali MF, Legare ME, Tjalkens RB (2017) Microglia amplify inflammatory activation of astrocytes in manganese neurotoxicity. J Neuroinflamm 14:99.

Kucharova K, Stallcup WB (2010) The NG2 proteoglycan promotes oligodendrocyte progenitor proliferation and developmental myelination. Neuroscience 166:185-194.

Lam JK, Chow MY, Zhang Y, Leung SW (2015) siRNA versus miRNA as therapeutics for gene silencing. Mol Ther Nucleic Acids 4:e252.

Lee S, Leach MK, Redmond SA, Chong SYC, Mellon SH, Tuck SJ, Feng ZQ, Corey JM, Chan JR (2012) A culture system to study oligodendrocyte myelination-processes using engineered nanofibers. Nat Methods 9:917-922.

Li N, Leung GK (2015) Oligodendrocyte precursor cells in spinal cord injury: a review and update. Biomed Res Int 2015:20.

Livak KJ, Schmittgen TD (2001) Analysis of relative gene expression data using real-time quantitative PCR and the 2−ΔΔCT method. Methods 25:402-408.

Loane DJ, Byrnes KR (2010) Role of microglia in neurotrauma. Neurotherapeutics 7:366-377.

Lu QR, Yuk D, Alberta JA, Zhu Z, Pawlitzky I, Chan J, McMahon AP, Stiles CD, Rowitch DH (2000) Sonic hedgehog-regulated oligodendrocyte lineage genes encoding bHLH proteins in the mammalian central nervous system. Neuron 25:317-329.

Lull ME, Block ML (2010) Microglial activation and chronic neurodegeneration. Neurotherapeutics 7:354-365.

Markiewicz I, Lukomska B (2006) The role of astrocytes in the physiology and pathology of the central nervous system. Acta Neurobiol Exp 66:343-358.

Milbreta U, Lin J, Pinese C, Ong W, Chin JS, Shirahama H, Mi R, Williams A, Bechler ME, Wang J, ffrench-Constant C, Hoke A, Chew SY (2018) Scaffold-mediated sustained, non-viral delivery of miR-219/miR-338 promotes CNS remyelination. Mol Ther 27:411-423.

Nesic O, Xu G-Y, McAdoo D, Westlund High K, Hulsebosch C, Perez-Polo R (2001) IL-1 receptor antagonist prevents apoptosis and Caspase-3 activation after spinal cord injury. J Neurotrauma 18:947-956.

Nguyen LH, Gao M, Lin J, Wu W, Wang J, Chew SY (2017) Three-dimensional aligned nanofibers-hydrogel scaffold for controlled non-viral drug/gene delivery to direct axon regeneration in spinal cord injury treatment. Sci Rep 7:42212.

Orihuela R, McPherson CA, Harry GJ (2016) Microglial M1/M2 polarization and metabolic states. Brit J Pharmacol 173:649-665.

Parmentier-Batteur S, Finger EN, Krishnan R, Rajapakse HA, Sanders JM, Kandpal G, Zhu H, Moore KP, Regan CP, Sharma S, Hess JF, Williams TM, Reynolds IJ, Vacca JP, Mark RJ, Nantermet PG (2011) Attenuation of scratch-induced reactive astrogliosis by novel EphA4 kinase inhibitors. J Neurochem 118:1016-1031.

Stroncek JD, Reichert WM (2008) Overview of Wound Healing in Different Tissue Types. In: Indwelling neural implants: strategies for contending with the in vivo environment (Reichert WM, ed). Boca Raton FL: Taylor & Francis Group, LLC.

van der Goes A, Dijkstra CD (2001) Models for demyelination. Prog Brain Res 132:149-163.

Wang H, Moyano AL, Ma Z, Deng Y, Lin Y, Zhao C, Zhang L, Jiang M, He X, Ma Z, Lu F, Xin M, Zhou W, Yoon SO, Bongarzone ER, Lu QR (2017) miR-219 cooperates with miR-338 in myelination and promotes myelin repair in the CNS. Dev Cell 40:566-582.e565.

Wang K, Luo Y, Huang S, Yang H, Liu B, Wang M (2015) Highly fluorescent polycaprolactones decorated with di(thiophene-2-yl)-diketopyrrolopyrrole: A covalent strategy of tuning fluorescence properties in solid states. J Polym Sci Pol Chem 53:1032-1042.

Wang YC, Li Y, Yang XZ, Yuan YY, Yan LF, Wang J (2009) Tunable thermosensitivity of biodegradable polymer micelles of poly(ε-caprolactone) and polyphosphoester block copolymers. Macromolecules 42:3026-3032.

Zamanian JL, Xu L, Foo LC, Nouri N, Zhou L, Giffard RG, Barres BA (2012) Genomic analysis of reactive astrogliosis. J Neurosci 32:6391-6410.

Zhang JM, An J (2007) Cytokines, inflammation and pain. Int Anesthesiol Clin 45:27-37.

Zhao X, He X, Han X, Yu Y, Ye F, Chen Y, Hoang T, Xu X, Li H, Xin M, Wang F, Appel B, Lu QR (2010) MicroRNA-mediated control of oligodendrocyte differentiation. Neuron 65:612-626.

Zhou Q, Wang S, Anderson DJ (2000) Identification of a novel family of oligodendrocyte lineage-specific basic helix-loop-helix transcription factors. Neuron 25:331-343.

C-Editors: Zhao M, Li CH; T-Editor: Jia Y

Additional Table 1 Sequences of primers for real time-PCR

	Gene		Sequence (5'-3')	Product size (bp)
1	**GAPDH**	Forward	TCTCTGCTCCTCCCTGTTCT	104
		Reverse	TACGGCCAAATCCGTTCACA	
2	**18S**	Forward	GCAATTATTCCCCATGAACG	123
		Reverse	GGCCTCACTAAACCATCCAA	
3	**RPL13A**	Forward	GTGGTGGTTGTACGCTGTGA	107
		Reverse	CGAGACGGGTTGGTGTTCAT	
4	**Sox6**	Forward	AATGGCGAGGATGAAATGGAAG	117
		Reverse	GCAAACAAAAGCTCCTCAGTTG	
5	**Hes5**	Forward	ATGCGTCGGGACCGCATCAAC	150
		Reverse	GGCGAAGGCTTTGCTGTGCTTC	
6	**PDGFR-α**	Forward	GTTGGAGCTTGAGGGAGTGAA	91
		Reverse	AAAATCCGATAGCCCGGAGG	
7	**FoxJ3**	Forward	CAACCTTCCAGAACGAGATAAA	703
		Reverse	TGCTAGGAGAGTGCTGATAG	
8	**ZFP238**	Forward	TGAAGACGAAGGCGAAGATGAC	173
		Reverse	AGGGGCTGGCTACTGTTTTTCC	
9	**TNF-α**	Forward	CCACACCGTCAGCCGATT	81
		Reverse	TCCTTAGGGCAAGGGCTCTT	
10	**IL-1α**	Forward	ACATCCGTGGAGCTCTCTTTACA	87
		Reverse	TTAAATGAACGAAGTGAACAGTACAGATT	
11	**IL-1β**	Forward	GCTGTGGCAGCTACCTATGTCTTG	120
		Reverse	AGGTCGTCATCATCCCACGAG	
12	**GFAP**	Forward	TGGCCACCAGTAACATGCAA	134
		Reverse	CAGTTGGCGGCGATAGTCAT	
13	**Vimentin**	Forward	GCGAGAGAAATTGCAGGAGGA	111
		Reverse	CGTTCAAGGTCAAGACGTGC	
14	**Serpina3**	Forward	CTCTCAGGTGGTCCACAAGG	107
		Reverse	GAGGGTACAGTTTCGCAGACA	
15	**Olig2**	Forward	TAACTCTTTGGCTGAACGAACA	183
		Reverse	CAGTGCTCTGCGTCTCTTCTAA	
16	**NG2**	Forward	GTTGCTCTGGGGTTGGTTAATT	90
		Reverse	CCATATACTCCAGGGCTTCCAT	
17	**CNP**	Forward	ATGCCCAACAGGATGTGGTG	154
		Reverse	GATGAGGGCTTGTCCAGGTC	
18	**MBP**	Forward	TTCTTTAGCGGTGACAGGGGTG	123
		Reverse	GACTACTGGGTTTTCATCTTGGGTC	
19	**MAG**	Forward	ACAGCGTCCTGGACATCATCAACA	85
		Reverse	ATGCAGCTGACCTCTACTTCCGTT	

CNP: 2',3'-Cyclic nucleotide 3'-phosphodiesterase; GAPDH: glyceraldehyde-3-phosphate dehydrogenase; GFAP: glial fibrillary acidic protein; IL: interleukin; MAG: myelin-associated glycoprotein; MBP: myelin basic protein; NG2: neural/glial antigen 2; Olig2: oligodendrocyte transcription factor; PDGFR: platelet-derived growth factor receptor; TNF: tumor necrosis factor.